Int. J. Heat Mass Transfer. Vol. 36, No. 7, pp. 1883–1895, 1993
Printed in Great Britain

0017-9310/93 $6.00+0.00

Measurements of laminar mixed convection in boundary-layer flow over horizontal and inclined backward-facing steps

H. I. ABU-MULAWEH, B. F. ARMALY and T. S. CHEN

Department of Mechanical and Aerospace Engineering and Engineering Mechanics, University of Missouri–Rolla, Rolla, MO 65401, U.S.A.

(*Received* 27 *April* 1992 *and in final form* 10 *August* 1992)

Abstract—Measurements and predictions of velocity and temperature distributions are presented for buoyancy-assisting mixed convection laminar boundary-layer flow over horizontal and inclined, two-dimensional backward-facing steps. Laser–Doppler velocimeter and cold wire anemometer are used to measure simultaneously the velocity and the temperature distributions, respectively. Flow visualizations are carried out to determine the reattachment length and the onset/start of vortex instability for different wall temperatures ($0°C \leqslant \Delta T \leqslant 30°C$), free stream velocities ($0.285\ m\ s^{-1} \leqslant u_\infty \leqslant 0.7\ m\ s^{-1}$), step heights ($0.35\ cm \leqslant s \leqslant 0.8\ cm$), and inclination angles ($30° \leqslant \phi \leqslant 90°$) as measured from the vertical direction. For the horizontal case, the buoyancy force has a negligible effect on the velocity and temperature distributions, but it influences significantly the onset/start of instability. The inclination angle, on the other hand, affects significantly the temperature and velocity distributions. As the inclination angle from the vertical increases, the local Nusselt number decreases, while the reattachment length and the location of the maximum Nusselt number behind the backward-facing step increase.

INTRODUCTION

FLOW SEPARATION occurs in many heat transfer devices, such as heat exchangers, cooling systems for digital computers, combustion chambers, cooling passages of turbine blades, and chemical process equipments. Owing to its simple geometry, the flow separation behind a backward-facing step has been studied extensively. Fluid flow aspect over a backward-facing step has been studied by Armaly and Durst [1], Eaton and Johnson [2], Simpson [3] and Armaly *et al.* [4]. Others have studied the heat transfer aspect of this separated flow; for example, Aung [5, 6], Aung *et al.* [7], Vogel and Eaton [8], Sparrow and Chuck [9] and Sparrow *et al.* [10]. The majority of the previous investigations have been mainly numerical in nature and have dealt only with forced convection separated flow. Relatively fewer studies have been published on mixed convection in separated flows. Numerical results have also been reported on mixed convection flows by Branten and Patankar [11] and by Lin *et al.* [12, 13]. Recently, Baek *et al.* [14] and Abu-Mulaweh *et al.* [15] reported on measurements in mixed convection for separated boundary-layer flow downstream of a two-dimensional vertical backward-facing step for uniform wall temperature and for uniform wall heat flux cases, respectively. In addition, Cheng and Kimura [16] reported on a qualitative study, using flow visualization, of mixed convective instability for laminar boundary-layer flow over a horizontal backward-facing step.

The present study extends the experimental work of Baek *et al.* [14] to the inclined and horizontal backward-facing step geometry. Results of interest, such as velocity and temperature distributions, local Nusselt numbers, reattachment lengths, and onset/start of vortex instability, are reported to illustrate the effects of the inclination angle and the buoyancy force on these parameters.

EXPERIMENTAL APPARATUS AND PROCEDURE

The experimental study was carried out in an existing low-turbulence, open-circuit air tunnel which could be rotated and fixed at any desired inclination angle. Details of the air tunnel have been described by Ramachandran *et al.* [17], and a schematic diagram of the air tunnel is shown in Fig. 1. The test section of the tunnel consisted of a heated backward-facing step geometry, with an adiabatic upstream section (30.48 cm long), an adiabatic backward-facing step, and a heated (constant temperature) downstream section (79 cm long) behind the step. This test section and other instrumentations (laser–Doppler velocimeter and cold wire anemometer) have been described in detail by Baek *et al.* [14]. The heated wall, downstream from the step, was constructed from four layers which were held together by screws and instrumented to provide an isothermal heated surface. The upper layer (1.27 cm thick) was an aluminum plate instrumented with 18 copper–constantan thermo-

NOMENCLATURE

g	gravitational acceleration
Gr_s	Grashof number, $g\beta(T_W-T_\infty)s^3/\nu^2$
Gr_x	$Gr_s \cos\phi$
Gr_{xc}	critical Grashof number, $g\beta(T_W-T_\infty)x_c^3/\nu^2$
Gr_y	$Gr_s \sin\phi$
h	heat transfer coefficient, $-k(\partial T/\partial y)_{y=0}/(T_W-T_\infty)$
H	height of computational domain
k	thermal conductivity
Nu_s	local Nusselt number, hs/k
p	pressure
P	dimensionless pressure $(p+\rho gx\cos\phi+\rho gy\sin\phi)/(\rho u_\infty^2)$
Pr	Prandtl number, ν/α
Re_s	Reynolds numbers, $u_\infty s/\nu$
Re_x	local Reynolds number, $u_\infty x/\nu$
Re_{xc}	critical Reynolds number, $u_\infty x_c/\nu$
s	step height
T	fluid temperature
T_∞	free stream temperature
T_W	heated wall temperature
u	streamwise velocity component
u_∞	free stream velocity
U	dimensionless streamwise velocity component, u/u_∞
v	transverse velocity component
V	dimensionless transverse velocity component, v/u_∞
x, y	streamwise and transverse coordinates
X, Y	dimensionless streamwise and transverse coordinates, x/s, y/s
x_c	critical length for vortex instability
x_e	downstream heated length
x_i	inlet length upstream of the step
x_n	location of maximum Nusselt number
x_r	reattachment length
X_e, X_i, X_n, X_r	$x_e/s, x_i/s, x_n/s, x_r/s$.

Greek symbols

α	thermal diffusivity
β	volumetric expansion coefficient
δ_s	boundary layer thickness at the step, $5x_i/Re_{xi}^{1/2}$
ΔT	temperature difference (T_W-T_∞)
θ	dimensionless temperature $(T-T_\infty)/(T_W-T_\infty)$
ν	kinematic viscosity
ρ	density
ϕ	angle of inclination from the vertical.

couples that were distributed in both the axial and the transverse directions. Each thermocouple was inserted into a hole on the backside of the plate and its measuring junction was flush with the test surface. The second layer consisted of five separately controlled heater pads, and an insulation layer formed the third layer. The bottom layer was an aluminum plate which served as backing and support for the structure of the plate. The construction details of the heated wall have been presented by Ramachandran [18]. The upstream section of the backward-facing step was constructed from Plexiglas. The front edge of this upstream section was chamfered to provide a good starting edge for the boundary-layer flow, and the back edge was squared to form the adiabatic step. The height of the step could be changed to any desired value (0.35–0.8 cm). The free stream velocity in the tunnel could be varied between 0.25 and 3.0 m s^{-1} and the heated downstream plate could be maintained at a uniform and constant temperature (within 0.2°C) by controlling power input to the individual heaters.

The velocity at any desired location was measured by a three-beam, backward scattering, two-component laser–Doppler velocimeter (LDV) and a three-dimensional traversing system, as described by Baek *et al.* [14]. Glycerin smoke particles 2–5 μm in diameter, generated by immersing a 100 W heating element into a glycerin container, were mixed with the inlet air to provide the scattering particles for the LDV measurements and also for the flow visualizations. A 15 W collimated beam of high intensity white light, 2.5 cm in diameter, was used to visualize the flow and to determine the reattachment length and the onset of vortex instability. Temperature measurements were performed by utilizing a cold wire anemometer with a boundary-layer probe and a traversing system, as described by Ramachandran *et al.* [17]. The probe was calibrated frequently to ensure accurate temperature measurements. Velocity and temperature profiles were measured simultaneously by adjusting the cold wire probe to be about 2 mm behind the measuring volume of the LDV system. Rapid data aquisition and data reduction for measurements of both temperature and velocity were performed through a 12-bit analog to digital converter and software on an IBM AT microcomputer.

NUMERICAL ANALYSIS

The experimental geometry was modelled for numerical simulation, as shown in Fig. 2. The upstream portion of the stepped wall and the backward-facing step were considered as adiabatic, while the wall downstream of the step was considered as being heated to a uniform temperature T_W. The gravitational acceleration g is acting vertically downward.

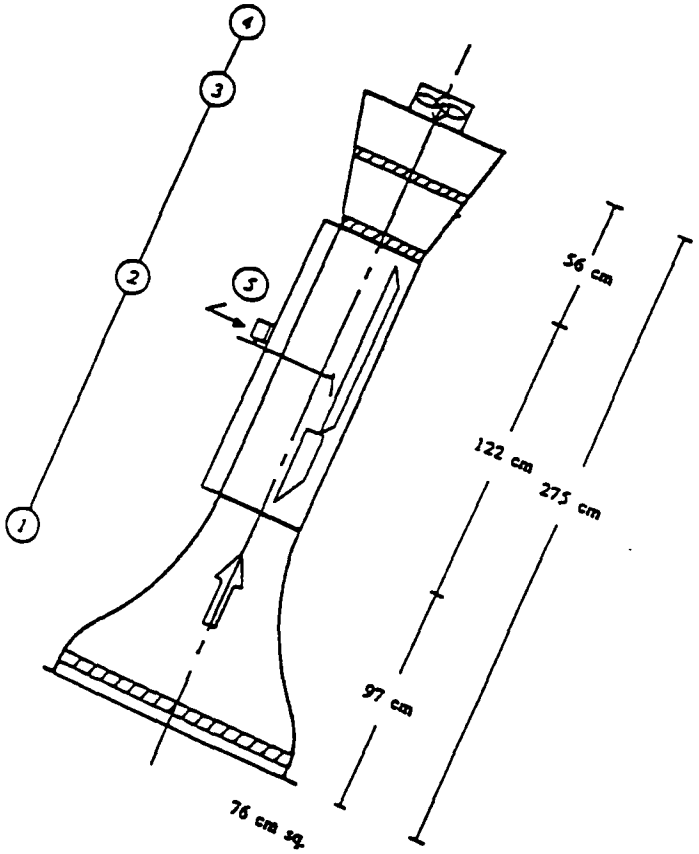

FIG. 1. Schematic diagram of air tunnel: 1, mixing chamber; 2, test section; 3, diffuser; 4, fan assembly; 5, probe traversing unit.

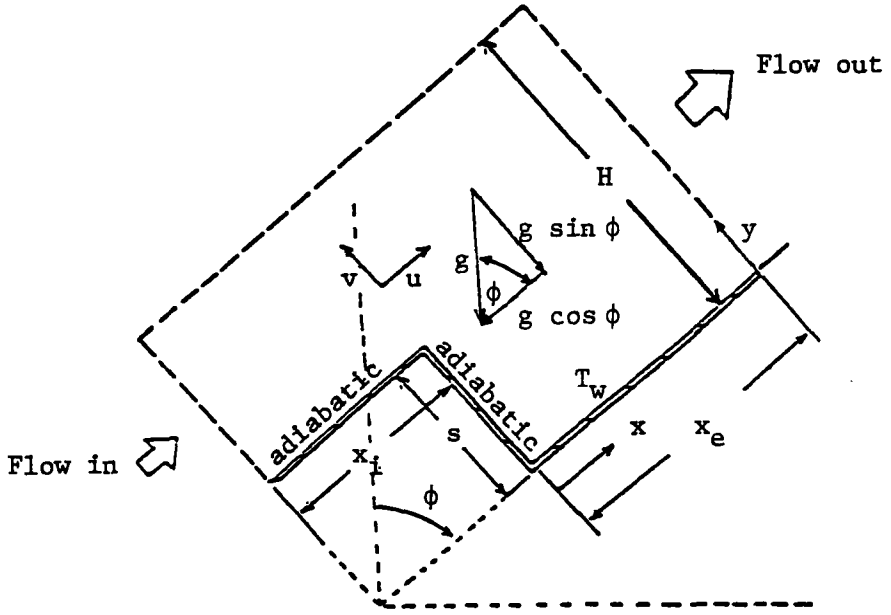

FIG. 2. Schematic diagram of the computation domain.

The thermal properties were considered to be constant but evaluated at the film temperature $T_f = (T_\infty + T_w)/2$.

By utilizing the Boussinesq approximation, the governing conservation equations for the physical problem under consideration can be written in non-dimensional form as follows:

$$\partial U/\partial X + \partial V/\partial Y = 0 \quad (1)$$

$$U\partial U/\partial X + V\partial U/\partial Y = -\partial P/\partial X + (1/Re_s)(\partial^2 U/\partial X^2 + \partial^2 U/\partial Y^2) + (Gr_x/Re_s^2)\theta \quad (2)$$

$$U\partial V/\partial X + V\partial V/\partial Y = -\partial P/\partial Y + (1/Re_s)(\partial^2 V/\partial X^2 + \partial^2 V/\partial Y^2) + (Gr_y/Re_s^2)\theta \quad (3)$$

$$U\partial\theta/\partial X + V\partial\theta/\partial Y = (1/Pr\,Re_s)(\partial^2\theta/\partial X^2 + \partial^2\theta/\partial Y^2). \quad (4)$$

The boundary conditions are given by

$1 < Y < H/s, \quad X = -X_i$:

$$U = 1, \quad V = \theta = 0 \quad \text{(at inlet)} \quad (5)$$

$0 < Y < H/s, \quad X = X_e$:

$$\partial^2 U/\partial X^2 = \partial^2 V/\partial X^2 = \partial^2\theta/\partial X^2 = 0 \quad \text{(at exit)} \quad (6)$$

$Y = H/s, \quad -X_i < X < X_e$:

$$U = 1, \quad \partial V/\partial Y = 0, \quad \theta = 0 \quad \text{(free stream)} \quad (7)$$

$Y = 1, \quad -X_i < X < 0$:

$$U = V = 0, \quad \partial\theta/\partial Y = 0 \quad \text{(upstream wall)} \quad (8)$$

$0 < Y < 1, \quad X = 0$:

$$U = V = 0, \quad \partial\theta/\partial X = 0 \quad \text{(step wall)} \quad (9)$$

$Y = 0, \quad 0 < X < X_e$:

$$U = V = 0, \quad \theta = 1 \quad \text{(downstream wall)}. \quad (10)$$

The upstream length x_i, the downstream length x_e, the height of the calculation domain H, and the step height s were chosen to be 30.48, 40.0, 15.0 and 0.35–8.0 cm, respectively. The horizontal case corresponds to $\phi = 90°$, with Gr_x equal to zero and Gr_y equal to Gr_s. Results for the vertical case (i.e. $\phi = 0°$), where $Gr_y = 0$ and $Gr_x = Gr_s$, have been reported by Baek *et al.* [14]. The governing set of coupled partial differential equations was solved by using a finite-difference scheme using the SIMPLE algorithm, as described by Patankar [20]. The solution procedure starts with the initial estimates for velocities, temperatures and pressure fields, along with the physical boundary conditions, and an iteration is performed until a converged solution is obtained. The momentum equations are used first in the iteration process, using the estimated temperature for the buoyancy force calculations, and then the energy equation is solved to upgrade the temperature. This process is repeated for each iteration step until a converged solution is obtained. Convergence of the solution is considered satisfactory when the normalized sum of residuals (mass, momentum and energy) over the whole calculation domain is less than 0.01.

A non-uniform grid distribution was used in the computations, in both the streamwise and the transverse coordinates. A large number of grid points were used adjacent to the walls in the y coordinate direction and near the step and the reattachment point in the x coordinate direction, where large variations of velocities were detected from measurements. Solutions were performed with different grid densities and grid numbers to ensure a grid-independent solution. A grid density of $N_x \times N_y = 100 \times 80$ was found to be sufficient in providing a grid-independent solution. For two mesh sizes of 100×80 and 140×120, the maximum changes in the predicted velocity, Nusselt number and reattachment length were less than 3, 1.5 and 1%, respectively. The computations were performed on an Apollo 10000 computer and required 1000–1500 iterations in most cases to reach a converged solution.

RESULTS AND DISCUSSION

The development of the boundary-layer flow and its two-dimensional nature was verified through flow visualizations and through measurements of velocity and temperature across the width of the air tunnel, at various heights above the test surface. These measurements displayed a wide region, about 80%, around the center of the tunnel's width where the flow can be approximated (to within 5%) as being two-dimensional. All reported streamwise velocity and temperature distributions in the transverse, y, direction were taken along the midplane ($z = 0$) of the plate's width, and only after the system had reached steady state conditions.

A. *Horizontal case*

Figure 3 presents the measured and predicted streamwise velocity distributions for pure forced convection flow ($T_w - T_\infty = 0°C$) at four different streamwise locations ($X = 2.31$, 4.62, 9.23 and 36.9) for the case of step height $s = 0.65$ cm and free stream velocity $u_\infty = 0.465$ m s^{-1}. The figure indicates that good agreement exists between measured and predicted results (within 5%). As can be seen from the figure, negative velocities exist in the profiles at $X = 2.31$ and 4.62, indicating that these locations are upstream of the reattachment point and inside the recirculation region behind the step.

The effect of buoyancy forces (i.e. heating the wall downstream from the step) on the streamwise velocity distributions at four different streamwise locations ($X = 2.31$, 4.62, 9.23 and 36.9) are illustrated in Fig. 4 for the case of step height $s = 0.65$ cm, free stream velocity of $u_\infty = 0.465$ m s^{-1}, and four different temperature differences ($T_w - T_\infty = 0$, 5, 15 and 30°C). This figure indicates clearly that the wall heating has only a small effect on the streamwise velocity dis-

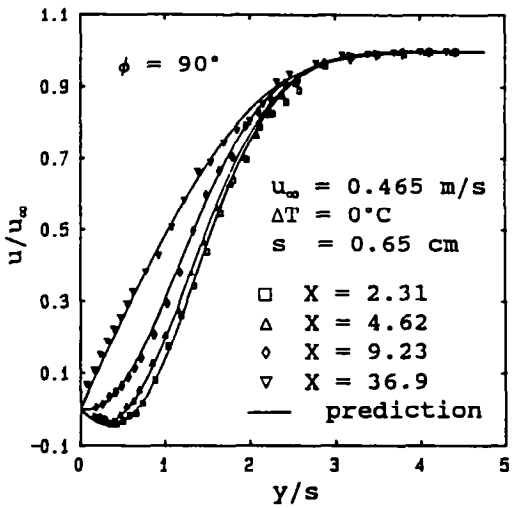

FIG. 3. Dimensionless axial velocity distribution (uncertainty in u/u_∞ is ± 0.014 and in y/s is ± 0.022).

tributions when the flow is stable and two-dimensional. This behavior is in sharp contrast with the cases of vertical [14] and inclined backward-facing step flows, where the buoyancy force affects significantly the streamwise velocity distributions. In these cases, however, the buoyancy force has a non-zero component in the streamwise direction in comparison to the horizontal case where the buoyancy force component in the streamwise direction is zero. Figure 4 also shows that the measured values agree favorably well with predictions (within 5%) except for the case of $(T_w - T_\infty) = 30°C$ at $X = 36.9$, where the flow is no longer laminar or two-dimensional due to the onset of vortex instability. This instability is similar to what has been observed by Moharreri *et al.* [19] adjacent to a horizontal plate in mixed convection. Figure 5 was prepared to illustrate the effect of free stream velocities ($u_\infty = 0.285$ and 0.465 m s^{-1}) on the velocity distributions at a streamwise location of $X = 9.23$ for a fixed temperature difference $(T_w - T_\infty)$ of 15°C. This figure illustrates that for these conditions the velocity gradient at the wall is higher for the lower free stream velocity which is due to the changes in the reattachment length, i.e. a higher velocity is also associated with a larger reattachment length.

Figure 6 presents the measured and the predicted temperature distributions at four different streamwise locations ($X = 2.31$, 4.62, 9.23 and 36.9) for the case of step height $s = 0.65$ cm and free stream velocity $u_\infty = 0.465$ m s^{-1}, for three different temperature differences ($T_w - T_\infty = 5$, 15 and 30°C). Similar to the velocity distributions in Fig. 4, the buoyancy force (wall heating) has a negligible effect on the temperature distributions when the flow is stable and two-dimensional. The measurements agree well with numerical predictions (within 5%) except for the case of $(T_w - T_\infty) = 30°C$ at $X = 36.9$, where the flow is no longer laminar and two-dimensional because of the onset of vortex instability. Figure 7 shows the effect of free stream velocities ($u_\infty = 0.285$ and 0.465 m s^{-1}) on the temperature distribution at three downstream locations ($X = 2.31$, 4.62, 9.23) for a fixed temperature difference $(T_w - T_\infty)$ of 15°C. This figure illustrates that the temperature gradient at the heated wall in the recirculation region ($X = 2.31$) for the conditions presented is lower for the higher free stream velocity (due to changes in reattachment length and size of recirculation region), but the reverse trend is observed downstream of the reattachment point ($X \geqslant 4.62$).

Figure 8 illustrates the effects of the wall temperature on the axial variation of the local Nusselt number for the case of a step height $s = 0.65$ cm, for three different temperature differences $(T_w - T_\infty) = 5$, 15 and 30°C, and two free stream velocities $u_\infty = 0.285$ and 0.465 m s^{-1}. As can be seen from the figure, measurements agree favorably with numerical predictions (within 8%). For a given free stream velocity, the local Nusselt number is only slightly affected by increasing the wall temperature. The results illustrate, however, that a lower free stream velocity produces a higher Nusselt number in the recirculation region for the conditions presented. This is due mainly to the changes in the size of the recirculation region and the reattachment length. The experimental results for the cases of $u_\infty = 0.465$ m s^{-1} with $T_w - T_\infty = 30°C$ and $u_\infty = 0.285$ m s^{-1} with $T_w - T_\infty = 15°C$ are confined to smaller streamwise locations than the other cases because vortex instability develops for these conditions beyond that streamwise location.

Flow visualizations were carried out to determine the reattachment length and the onset of vortex instability for different inlet air velocities, step heights, and wall free stream temperature differences. As stated earlier, the wall heating (buoyancy force) does not affect the reattachment length but does affect the onset of vortex instability. The reattachment length observations are limited to the region where the flow is laminar and two-dimensional, i.e. prior to the onset of vortex instabilities which normally make the flow three-dimensional. The measured reattachment lengths for the different flow velocities and step heights in this study can be correlated, to within 15%, by

$$X_r = 0.023(\delta_s/s)Re_s + f(s/x_i) = 0.023[5(x_i/s)Re_{x_i}^{-1/2}]Re_s + f(s/x_i) \quad (11)$$

where

$$f(s/x_i) = 8995.8(s/x_i)^2 - 114.2(s/x_i) - 3.4. \quad (12)$$

The step height and the Reynolds number range used in establishing this correlation are $0.35 < s < 0.8$ cm and $50 < Re_s < 300$. The reattachment length, and hence the size of the recirculation region, increases as the free stream velocity or the step height increases. This is the same correlation that was established by Abu-Mulaweh *et al.* [15] for the vertical backward-facing step under isothermal flow conditions.

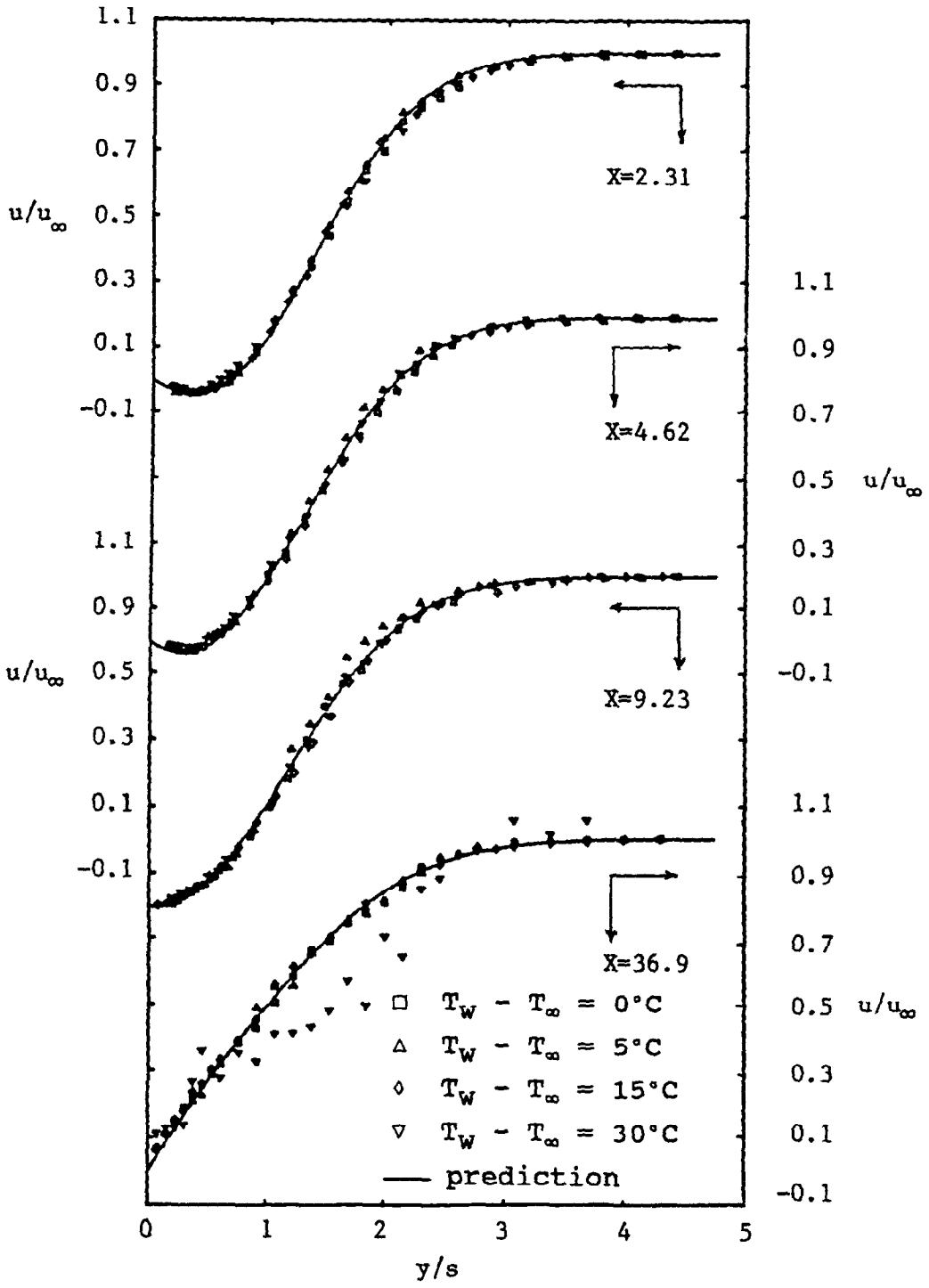

FIG. 4. Effects of wall temperature on the velocity distribution for $u_\infty = 0.465$ m s^{-1}, $s = 0.65$ cm, and $\phi = 90°$ (uncertainty in u/u_∞ is ± 0.014 and in y/s is ± 0.022).

The onset of vortex instability limits the applicability of the two-dimensional laminar flow solution for predicting the flow and the heat transfer characteristics in this geometry. The critical length downstream of the step at which vortex instability (vortex rolls) starts to occur is affected by the free stream velocity, the step height, and the temperature difference between the heated wall and the free stream. Cheng and Kimura [16] reported that the longitudinal vortex rolls appear immediately behind the backward-

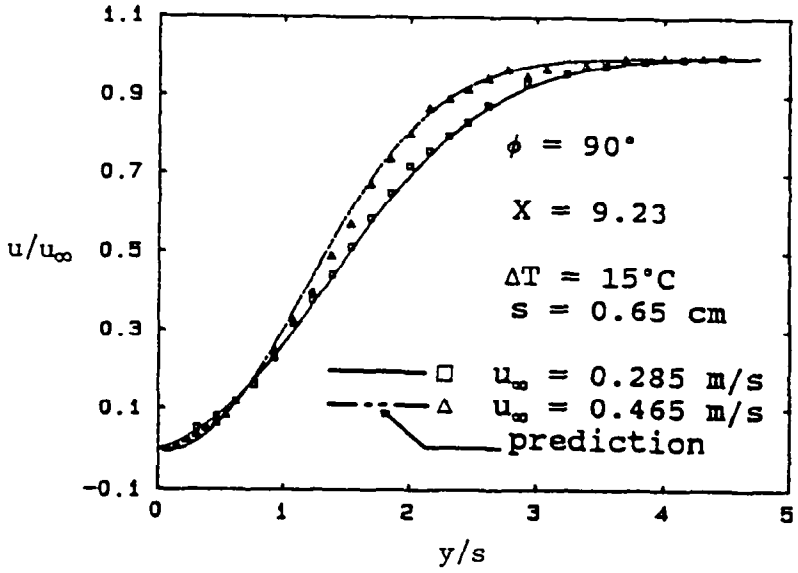

FIG. 5. Effects of free stream velocity on the velocity distribution (uncertainty in u/u_∞ is ± 0.014 and in y/s is ± 0.022).

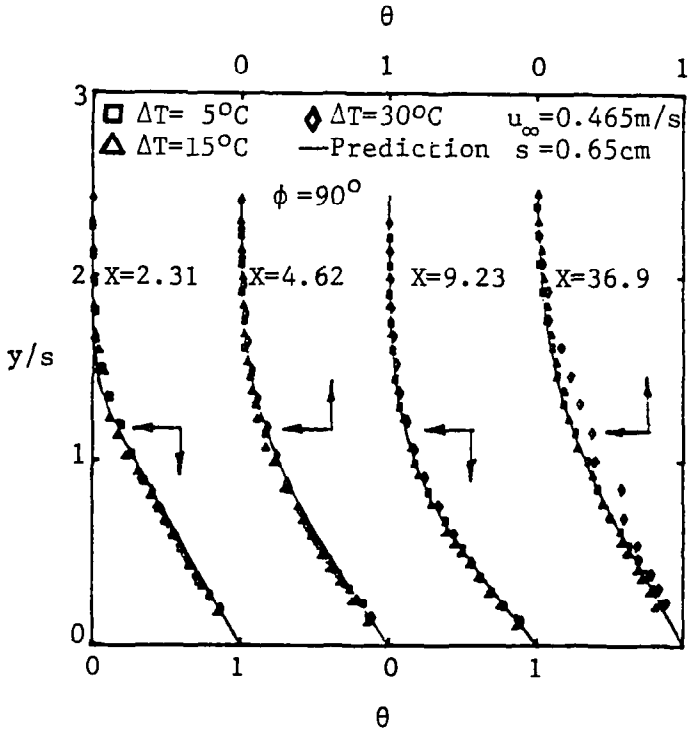

FIG. 6. Effects of wall temperature on the temperature distribution (uncertainty in y/s is ± 0.022 and in θ is ± 0.025).

facing step. This is due to the large step height that was used in their study ($s = 1.30$ cm), for which the flow appears to be unstable at any given heating condition or $(T_w - T_\infty)$. It was determined that for this experimental geometry with isothermal flow (i.e. no wall heating), the flow becomes unstable and the onset of instability occurs right behind the step when the step height is larger than $s = 1.0$ cm for a velocity

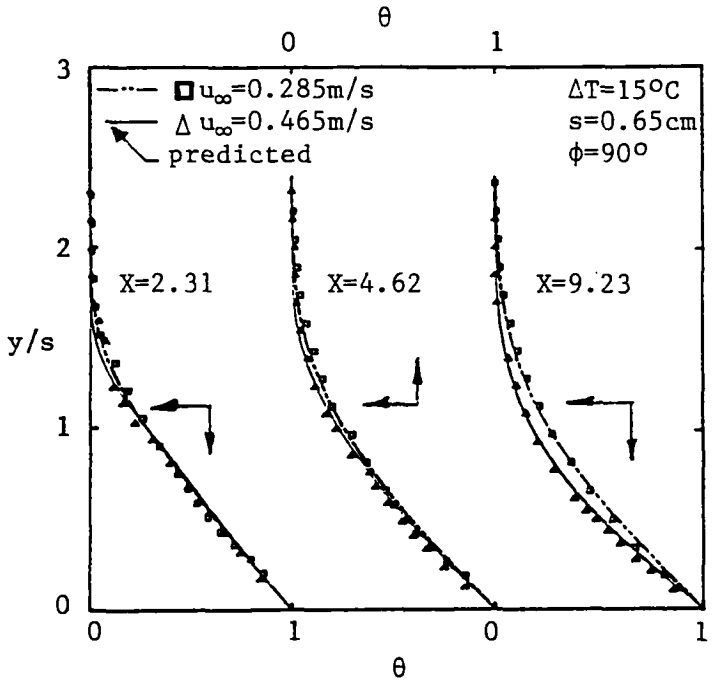

FIG. 7. Effects of free stream velocity on the temperature distribution (uncertainty in y/s is ± 0.022 and in θ is ± 0.025).

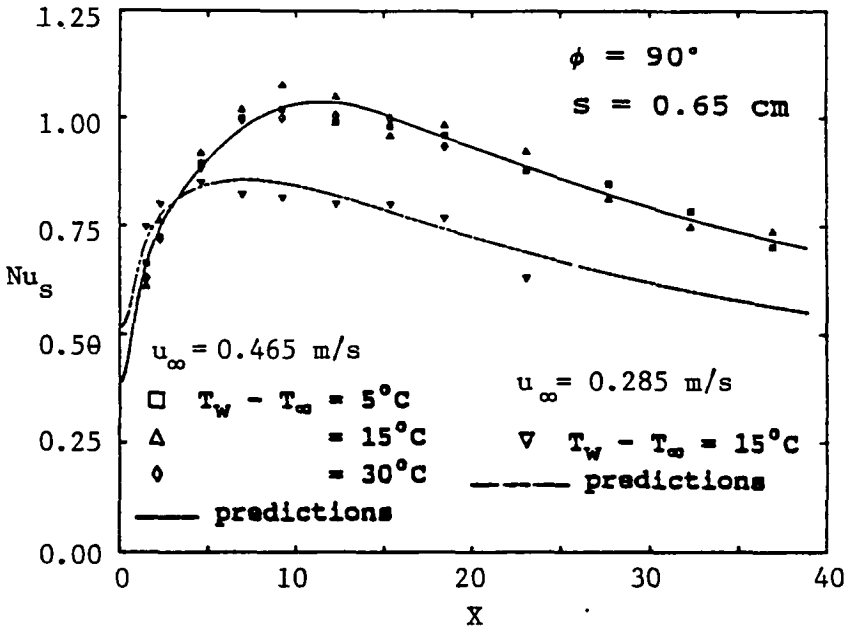

FIG. 8. Effects of buoyancy force on the axial variation of the Nusselt number (uncertainty in Nu_s is ± 0.05 and in X is ± 0.05).

higher than 0.285 m s^{-1}. For that reason, step heights smaller than 1.0 cm were used in determining the onset of vortex instability in this experiment. The axial locations where the onset of vortex instability occurs under different flow and heating conditions were correlated by the following equation as shown in Fig. 9:

$$Gr_{xc}/Re_{xc}^{2.5} = (s/\delta_s)^{2.25} \exp[f(Re_s)] \quad (13)$$

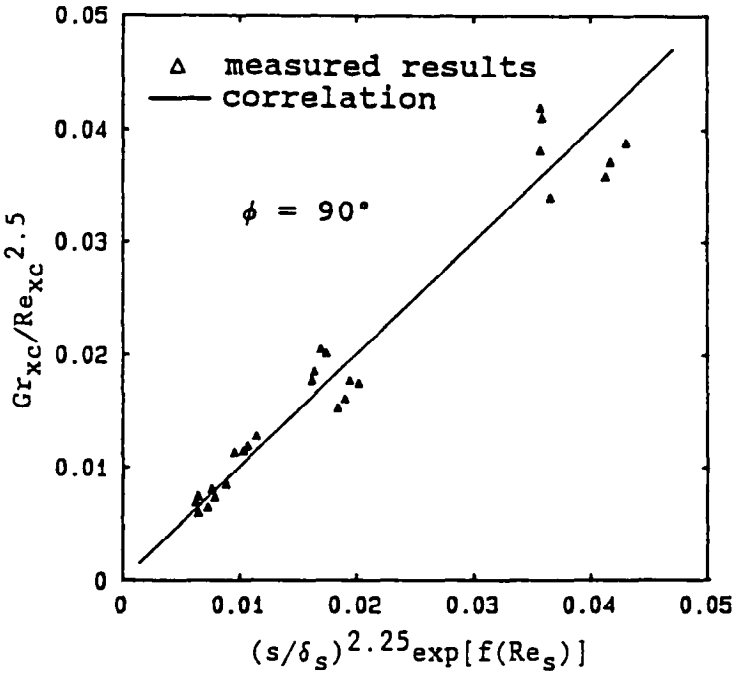

FIG. 9. Critical Grashof and Reynolds numbers for the onset of vortex instability.

where

$$f(Re_s) = 2.206\times10^{-4}Re_s^2 - 0.0896Re_s + 6.01. \quad (14)$$

The measured location for the onset of vortex instability x_c represents the average for several visual observations that were made under a fixed condition in order to reduce visualization errors. The location where the onset of vortex instability occurs could be reproduced experimentally to within 1 cm. The correlation predicts the measured location within a maximum error of 15%. The ranges of parameters used to establish the correlation equation (13) are listed below:

$$450 < Re_{xc} < 9715, \quad 7\times10^4 < Gr_{xc} < 6\times10^7$$

$$0.4 < s < 0.8\,\text{cm}, \quad 60 < Re_s < 230.$$

B. *Inclined case*

The tunnel along with the backward-facing step geometry was tilted and fixed at a given inclination angle to study the effect of inclination angle on the velocity and temperature distributions, and on the local Nusselt number. The step height, the free stream velocity and the wall temperature were fixed at $s = 0.7$ cm, $u_\infty = 0.58$ m s^{-1}, and $(T_W - T_\infty) = 10$°C, respectively. The only variable in this part of the study is the inclination angle ϕ which covered the values of 30, 45, 60 and 75°. The case of $\phi = 90$° corresponds to the horizontal orientation (discussed in the previous section) and the case of $\phi = 0$° corresponds to the vertical orientation which was reported by Baek *et al.* [14]. For the conditions of step height $s = 0.7$ cm, free stream velocity $u_\infty = 0.58$ m s^{-1}, and temperature difference $\Delta T = 10$°C, the flow remained laminar and two-dimensional throughout the entire length of the plate for all the inclination angles covered in this study. The measured and predicted streamwise velocity distributions are presented in Fig. 10 at three axial locations ($X = 2.5$, 5.0, 10.0) and for four inclination angles ($\phi = 30$, 45, 60, 75°). As can be seen from this figure, good agreement exists between the predicted and the measured values (within 5%). As the inclination angle ϕ increases from the vertical, the streamwise buoyancy force decreases, causing the velocity gradient at the wall in the recirculating region to increase in the negative sense.

The measured and predicted temperature distributions at three different downstream locations ($X = 2.5$, 5.0, 10.0) are presented in Fig. 11 for four inclination angles ($\phi = 30$, 45, 60, 75°). The values of $s = 0.7$ cm, $u_\infty = 0.58$ m s^{-1}, and $(T_W - T_\infty) = 10$°C result in $Re_s = 254$ and $Gr_s = 440$. It is evident from the figure that the numerical predictions are in good agreement with the experimental results (within 6%). The temperature gradient at the wall decreases as the inclination angle increases from the vertical due to a decrease in the buoyancy force.

The effects of the inclination angle on the axial variation of Nusselt number downstream of the step are illustrated in Fig. 12. For a given inclination angle, the Nusselt number at the heated wall increases from its minimum value at $X = 0$ to a maximum value at

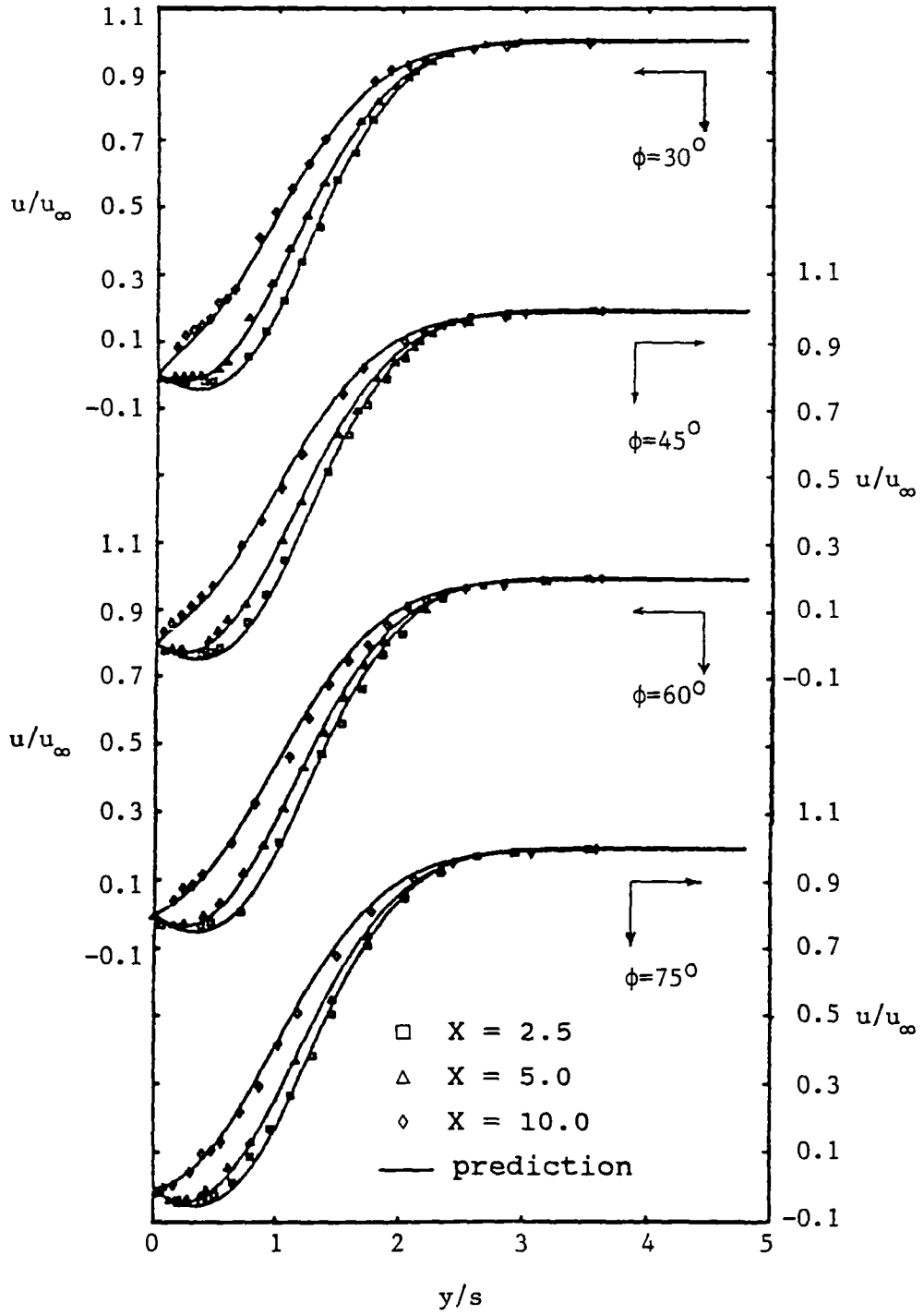

FIG. 10. Dimensionless axial velocity distributions for $u_\infty = 0.58$ m s^{-1}, $T_w - T_\infty = 10$°C, and $s = 0.7$ cm (uncertainty in u/u_∞ is ± 0.014 and in y/s is ± 0.022).

some distance downstream of the reattachment point, and then decreases slowly as the streamwise distance increases further. The local Nusselt number decreases as the inclination angle from the vertical increases due to a decrease in the temperature gradient at the heated wall. It can be seen that measurements agree favorably with numerical predictions (within 8%).

The reattachment lengths for different inclination angles ($\phi = 30, 45, 60, 75°$) were measured from flow visualizations. The uncertainty in these measurements

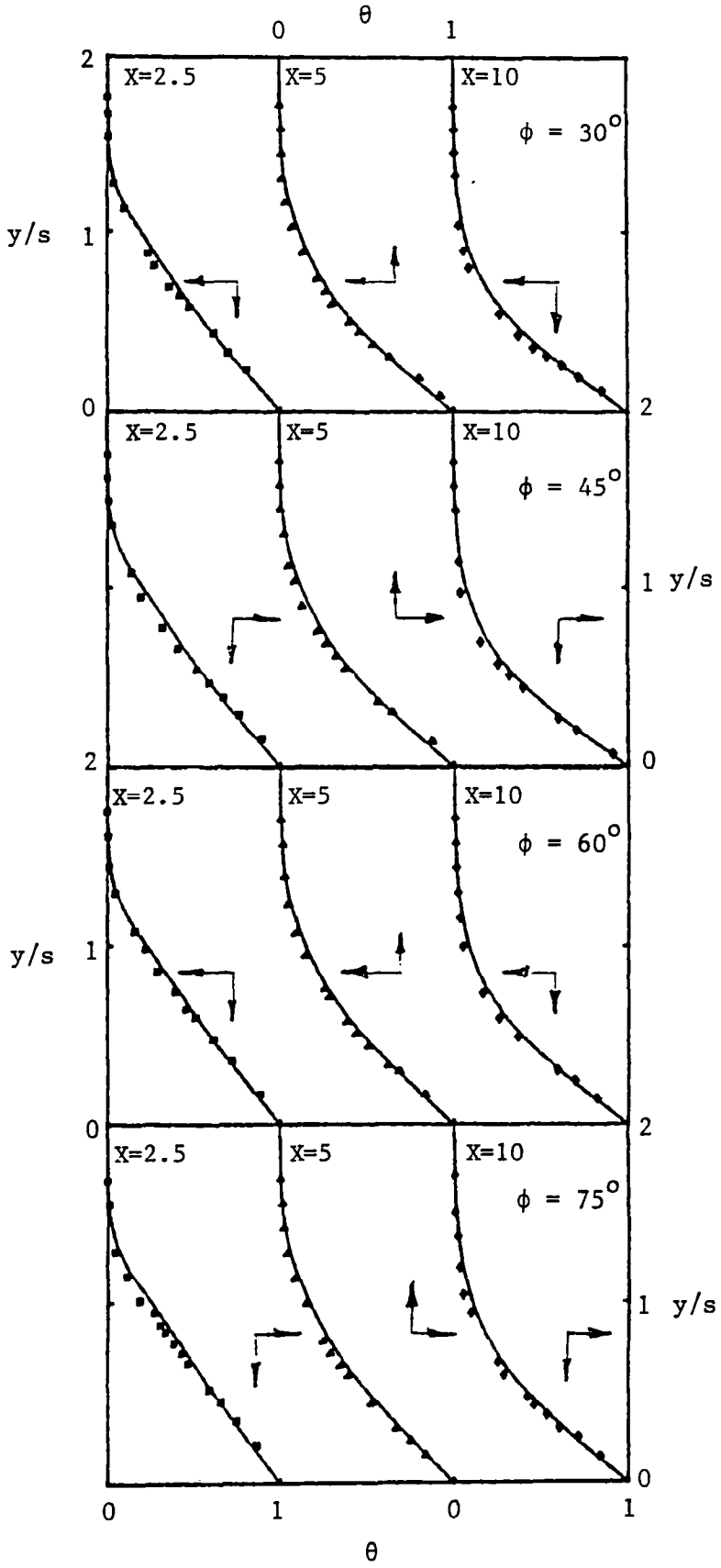

FIG. 11. Dimensionless temperature distributions for $u_\infty = 0.58$ m s^{-1}, $T_W - T_\infty = 10$°C, and $s = 0.7$ cm (uncertainty in y/s is ± 0.022 and in θ is ± 0.025).

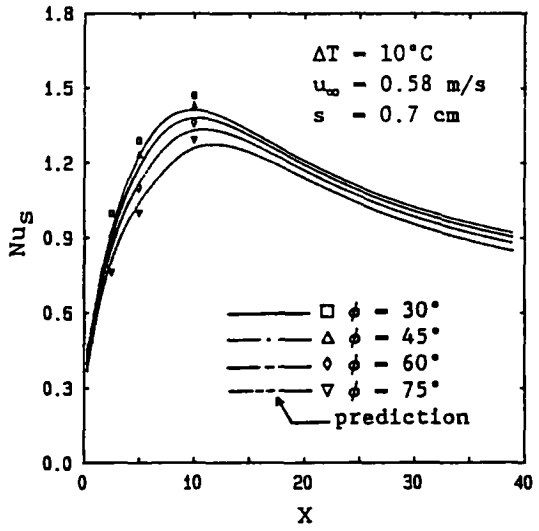

FIG. 12. Effects of inclination angle on the local Nusselt number (uncertainty in Nu_s is ± 0.05 and in X is ± 0.05).

is ± 1 mm, which is less than 5% of the smallest measured reattachment length. Figure 13 displays the predicted and measured behavior of the reattachment length X_r and the location where the Nusselt number reaches its maximum value, X_n, as a function of the inclination angle. An increase in the inclination angle ϕ from the vertical will cause an increase in the location of the maximum Nusselt number and the reattachment length due to a decrease in the streamwise buoyancy force. The maximum Nusselt number occurs downstream of the reattachment point (i.e. $X_n > X_r$) and the spacing between the maximum Nusselt number location and the reattachment point ($X_n - X_r$) decreases slowly as the inclination angle increases. A similar trend was reported by Lin *et al.* [13] for buoyancy-affected channel flows.

CONCLUSION

The results for the horizontal backward-facing step reveal that the buoyancy force resulting from heating the downstream wall has negligible effect on the velocity and the temperature fields, but it influences significantly the onset/start of vortex instability. A correlation was developed for the onset of vortex instability and that should define the region where the two-dimensional laminar flow solution is applicable for this geometry. The results for the inclined backward-facing step reveal that an increase in the inclination angle from the vertical reduces the streamwise component of the buoyancy force which causes an increase in the velocity gradient and a decrease in the temperature gradient at the wall in the recirculating region. It also increases the reattachment length X_r but decreases the local Nusselt number. Experimental results are found to be in good agreement with the predictions.

Acknowledgements—The present study was supported by a grant from the National Science Foundation (NSF CTS-

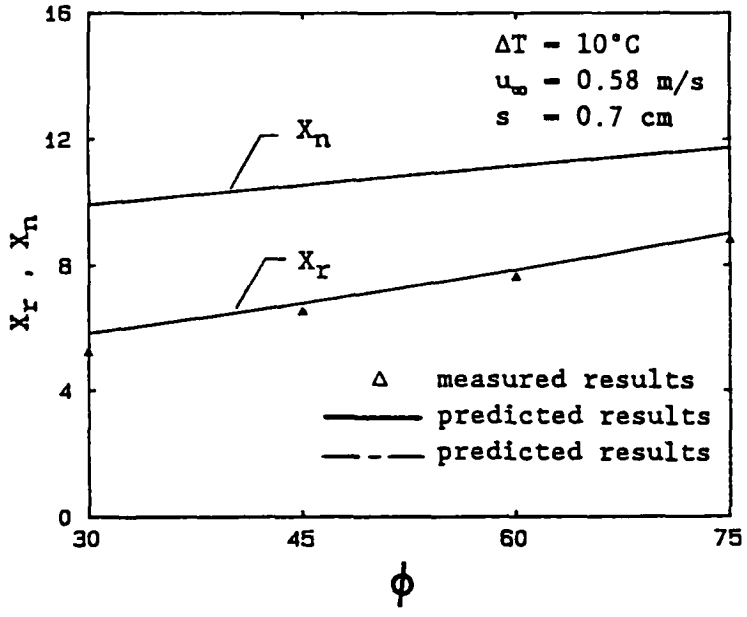

FIG. 13. Effects of inclination angle on the reattachment length and the location of maximum Nusselt number (uncertainty in X_r and X_n is ± 0.05 and in ϕ is $\pm 0.5°$).

8923010). Mr Bin Hong assisted in the numerical computations.

REFERENCES

1. B. F. Armaly and F. Durst, Reattachment length and recirculation regions downstream of two dimensional single backward facing step, *ASME HTD* **13,** 1–7 (1980).
2. J. K. Eaton and J. P. Johnson, A review of research on subsonic turbulent flow reattachment, *AIAA J.* **10,** 732–741 (1981).
3. R. L. Simpson, A review of some phenomena in turbulent flow separation, *J. Fluid Engng* **103,** 520–530 (1981).
4. B. F. Armaly, F. Durst, J. C. F. Pereira and B. Schonung, Experimental and theoretical investigation of backward-facing step flow, *J. Fluid Mech.* **127,** 473–496 (1983).
5. W. Aung, An experimental study of laminar heat transfer downstream of backsteps, *J. Heat Transfer* **105,** 823–829 (1983).
6. W. Aung, Separated forced convection, *Proc. ASME/JSME Thermal Engng Joint Conf.*, Vol. 2, pp. 499–515 (1983).
7. W. Aung, A. Baron and F. K. Tsou, Wall independence and effect of initial shear-layer thickness in separated flow and heat transfer, *Int. J. Heat Mass Transfer* **28,** 1757–1771 (1985).
8. J. C. Vogel and J. K. Eaton, Combined heat and fluid dynamics measurements downstream of a backward-facing step, *J. Heat Transfer* **107,** 922–929 (1985).
9. E. M. Sparrow and W. Chuck, PC solutions for heat transfer and fluid flow downstream of an abrupt asymmetric enlargement in a channel, *Numer. Heat Transfer* **12,** 19–40 (1987).
10. E. M. Sparrow, S. S. Kang and W. Chuck, Relation between the points of flow reattachment and maximum heat transfer for regions of flow separation, *Int. J. Heat Mass Transfer* **30,** 1237–1246 (1987).
11. M. E. Branten and S. V. Patankar, Analysis of laminar mixed convection in shrouded arrays of heated rectangular blocks, *Int. J. Heat Mass Transfer* **28,** 1699–1709 (1985).
12. J. T. Lin, B. F. Armaly and T. S. Chen, Mixed convection in buoyancy-assisting vertical backward-facing step flows, *Int. J. Heat Mass Transfer* **33,** 2121–2132 (1990).
13. J. T. Lin, B. F. Armaly and T. S. Chen, Mixed convection heat transfer in inclined backward-facing step flows, *Int. J. Heat Mass Transfer* **34,** 1568–1571 (1991).
14. B. J. Baek, B. F. Armaly and T. S. Chen, Measurements in buoyancy-assisting separated flow behind a vertical backward-facing step, *J. Heat Transfer* (in press).
15. H. I. Abu-Mulaweh, B. F. Armaly and T. S. Chen, Measurements in buoyancy-assisting laminar boundary-layer flow over a vertical backward-facing step—Uniform wall heat flux case, *Int. J. exp. Heat Transfer, Thermodynamics, Fluid Mech.* (in press).
16. K. C. Cheng and T. Kimura, Flow visualization experiments of convective instability phenomena in the laminar separation region downstream of a backstep with heating from below, *ASME HTD* **123,** 23–33 (1989).
17. N. Ramachandran, B. F. Armaly and T. S. Chen, Measurements and predictions of laminar mixed convection flows adjacent to a vertical surface, *J. Heat Transfer* **107,** 636–641 (1985).
18. N. Ramachandran, Measurements and predictions of laminar mixed convection from flat surfaces, MS Thesis, University of Missouri–Rolla (1983).
19. S. S. Moharreri, B. F. Armaly and T. S. Chen, Measurements in the transition vortex flow regime of mixed convection above a horizontal heated plate, *J. Heat Transfer* **110,** 358–365 (1988).
20. S. V. Patankar, *Numerical Heat Transfer and Fluid Flow.* Hemisphere, Washington, DC (1980).